JOURNAL OF CATALYSIS 133, 179–190 (1992)

Steady-State CO Oxidation Kinetics over the Pd(100) Single Crystal Surface and the $c(2 \times 2)$-Sn/Pd(100) Bimetallic Surface Alloy

A. DAVID LOGAN* AND MARK T. PAFFETT

Chemical & Laser Sciences Division Los Alamos National Laboratory Los Alamos, New Mexico 87545

Received March 6, 1991; revised June 7, 1991

The kinetic rates for CO oxidation have been measured on the surface of Pd(100) surface and the $c(2 \times 2)$-Sn/Pd(100) surface alloy ($\Theta_{Sn} = 0.5$ ML) in a high pressure/ultra-high vacuum surface analysis chamber over the temperature range of 443–673 K and the pressure range of 0.3–108 Torr. An Arrhenius activation energy of 22 kcal/mole was measured for CO oxidation at the Pd(100) single crystal surface. Furthermore, the reaction order for the CO was found to decrease from -0.2 to -0.9 as the pressure was lowered from 16 to 1 Torr CO ($P_{O2} = 8$ Torr), and the O_2 reaction order was found to increase from 0.6 to 1.0 at CO pressures of 16 and 1 Torr, respectively. These observations are in agreement with those previously reported for supported Pd/SiO_2 catalysts (Cant *et al., J. Catal.* **54,** 372 (1978)). These changes are attributed to the dramatic variation in heat of adsorption seen on the Pd(100) surface (34 to less than 20 kcal/mole at saturation coverage (nonlinear function)). The kinetic behavior of the $c(2 \times 2)$-Sn/Pd(100) bimetallic surface alloy was similarly studied and the activation energy for the CO oxidation reaction was found to be 12 kcal/mole. The $c(2 \times 2)$-Sn/Pd(100) surface alloy was ascertained to have catalytic reaction orders for CO and O_2 of 0.2 and 0.1, respectively. This is attributed to an increase in the oxygen surface coverage in the form of SnO_x ($x = 1-2$) atop the Pd(100) template. Possible roles that the SnO_x plays in accelerating this reaction are suggested. The surfaces were also characterized by Auger electron spectroscopy (AES), low energy electron diffraction (LEED), and thermal desorption mass spectroscopy (TDMS) prior to and following high pressure catalytic reactions.

1. INTRODUCTION

The study of CO oxidation over group VIII metals has been the subject of numerous studies and has applications in CO and O_2 gas scavenging in CO_2 lasers (*1*) and automotive exhaust pollution control (*2*). While these areas of application are quite distinct from one another, the common thread is the effective conversion of CO to CO_2. Furthermore, the mechanistic steps of adsorption, surface reaction, and desorption of the reactants and products involved in the CO oxidation reaction at well-defined surfaces (e.g., single crystals) have been thoroughly investigated by a combination of ultrahigh vacuum (UHV) and molecular beam surface science techniques. These results have been summarized in reviews by Engel and Ertl (*3, 4*). The role of bimetallic surfaces in facilitating this reaction is, however, much less clear. As a definitive test of the role that surface alloying has on the CO oxidation reaction, we have studied in this work the reactivity of the Pd(100) surface (perhaps the most studied metal for this reaction) and directly compared it to the reactivity of an ordered $c(2 \times 2)$-Sn/Pd(100) surface alloy.

The kinetic rate measurements have been made in the pressure regime 0.3–108 Torr using a microreactor technique coupled to a UHV surface analytical chamber and have a fundamental applicability to the real world technologies mentioned above. The preparation and characterization of this specific Sn/Pd(100) surface alloy has been recently accomplished by us using conventional UHV surface science techniques (*5*). We briefly summarize the pertinent aspects of the Sn/Pd(100) surface alloy in the following

*Present address: Research Staff, MD3179, Ford Motor Company, Dearborn, MI 48121.

0021-9517/92 $3.00

sections. The inherent advantages of examining heterogeneous surface reactivity of bimetallic catalytic materials using ultrathin ordered surface alloys and interfaces have been amply presented by various authors (*6, 7*). In the course of this study the reactivity of the $c(2 \times 2)$-Sn/Pd(100) surface alloy ($\theta_{CO} = 0.5$ ML) was determined to be superior to the clean Pd(100) surface at low temperatures ($T_s < 500$ K), and a molecular level description of the catalytic enhancement is suggested.

The oxidation of CO over Pd has been an extensively studied reaction on Pd films (*8–10*), Pd single crystals (*3, 4, 11*), and supported Pd catalysts (*12–16*). In general, single crystal and evaporated film Pd studies have been conducted at low pressures (i.e., below 10^{-5} Torr and 10^{-2} Torr, respectively). One notable exception is the work of Berlowitz *et al.* (*11*) who performed steady state CO oxidation over the Pd(110) single crystal surface at high pressures (24 Torr). In addition to these studies, model Pd catalysts have been characterized by surface science techniques at low pressures (*14*) and as supported catalysts at high pressures (310 to 0.15 Torr) (*12, 13, 17*). Except for the work of Palazov *et al.* (*17*), all of the studies have concluded that the reaction proceeds through a Langmuir–Hinshelwood (L–H) type mechanism involving reaction of chemisorbed carbon monoxide molecules and dissociatively adsorbed oxygen atoms. The CO desorption rate has been postulated to be the rate limiting step for most of the high pressure supported catalysts studies and low pressure single crystal studies (*3, 4, 11*). Furthermore, the observed activation energy for this reaction is thought to be dominated by the energetics of desorbing chemisorbed CO (*18*). Consequently, the partial pressure dependence of the reactants on this type of mechanism depends on the adsorption of O_2 at sites where CO has desorbed; thus leading to a first-order dependence in O_2 and a negative first-order dependence in CO (*3, 4, 11*).

Oxidation of CO has also been suggested to be a structure-insensitive reaction (*3, 14, 19*). Therefore, a great number of the activation energies reported in the literature should fall within a narrow range; however, the reported values for the activation energy for CO oxidation vary from 11 to 33 kcal/mole (*3, 4, 11–14, 20*) depending on the conditions of reaction and support. In fact, two notable exceptions of low activation energies of 14 and 11 kcal/mole are reported for high oxygen coverages on single crystal Pd(111) and Pd supported on SnO_2, respectively (*16, 20*). These low activation values are especially important in view of the high pressure (24 Torr) work of Berlowitz *et al.* who performed CO oxidation on the least close packed Pd single crystal surface (i.e., Pd(110)). This surface has the highest initial CO heat of adsorption (40 kcal/mole) (*21*). The Pd(100) surface readily adopts a compressed CO structure (*22*) that has a significantly lower heat of CO adsorption. Therefore, a comparison of the reactivity of the Pd(100) and the Pd(110) surfaces toward CO oxidation at higher pressures (24 Torr) will provide significant insight into the role of adsorbate bond strength (and hence the CO adsorbate structure) on this reaction.

The heat of adsorption of CO on palladium surfaces has been exhaustively measured and determined to vary significantly between the different low index planes as a function of coverage (*21, 22*). The CO adsorption process is considered nonactivated (e.g., $\Delta H_{ad} = E_{ad}$). For example, the CO heat of adsorption (ΔH_{ad}) values (noncompressed structure) on the Pd(111), Pd(110), and Pd(100) surfaces are 36 ($\theta_{CO} = 0.33$ ML), 32 ($\theta_{CO} = 0.5$ ML), and 30 ($\theta_{CO} = 0.5$ ML) kcal/mole, respectively. However, at slightly above $\theta_{CO} = 0.5$ ML on Pd(100) and Pd(111) surfaces there is a significant decrease in ΔH_{ad} for CO [i.e., $\approx$8 kcal/mole], while the Pd(110) surface has a ΔH_{ad} for CO near 32 kcal/mole. Ertl and Koch found that low pressure ($P_{total} < 4 \times 10^{-7}$ Torr) CO oxidation over the (100), (111), and (110) surfaces showed the same reaction rate and went through

a maximum at approximately 500 K, with lower rates of reactivity at higher temperatures (*19*). However, reactions run at high pressures (24 Torr) on the Pd(110) surface (*11*) did not display a rollover in reaction rate at higher temperatures. Given the limited data base for CO oxidation over Pd single crystal surfaces in the high (0.1–100 Torr) pressure regime, an examination of the reactivity of the Pd(100) surface toward CO oxidation is warranted.

Recently, in this laboratory, the production and UHV surface science characterization of Sn/Group VIII single crystal surface alloys has been undertaken (*5, 23, 24*). The basic procedure is to vapor deposit a specific initial concentration of Sn onto a specific single crystal substrate and to then follow the resultant surface stoichiometry and order as a function annealing temperature using Auger electron spectroscopy (AES) and low energy electron diffraction (LEED). Because of the inherently low surface free energy of Sn (and low melting temperature) in comparison to the Group VIII transition metal surfaces (*25*), the Sn adatoms diffuse across the surface and remain segregated at the outermost surface of the substrate. In addition, the formation of intermetallic compounds and ordered surface alloys is thermodynamically favorable (*26, 27*) at a high enough temperature. In all cases studied to date (e.g., the (100) and (111) faces of Pd, Ni, and Pt), the Sn vapor deposition and annealing step has produced ordered surface alloys in which the Sn adatoms are located approximately in the plane of the substrate surface (as opposed to an ordered metal overlayer). The extent of surface reconstruction and buckling has, however, only been explicitly determined for the Sn/Pt(111) system (*28*). In the context of CO oxidation, one of these specifically designed bimetallic surface alloys, the $c(2 \times 2)$-Sn/Pd(100) surface alloy (proposed ideal surface shown in Fig. 1) was chosen for two reasons. In our prior work (*5*), no CO adsorption was detected by TDMS on this surface following high vacuum exposures at

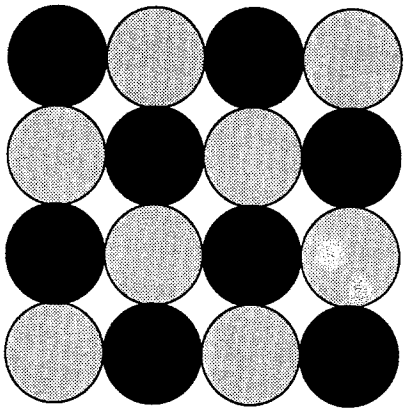

FIG. 1. Proposed ideal $c(2 \times 2)$-Sn/Pd(100) surface alloy structure.

room temperature; however, this surface displayed an enhancement in oxygen adsorption. The former observation is thought to be due to the elimination of Pd–Pd bridge sites that CO is known to exclusively occupy at all coverages on Pd(100) (*29*). Note that the Pd–Pd bridging sites have been completely disrupted in the proposed surface alloy structure of Fig. 1. Therefore, a study of CO oxidation at a surface that does not adsorb CO at temperatures above 300 K should provide an interesting contrast to the reactivity at the Pd(100) single crystal. It is also important to note that the under reaction conditions (P_i = 1–100 Torr, i = CO, O_2) the surface Sn component will exist in an oxidized state. The characterization of this oxygen-exposed surface has been previously examined (*5*) and is briefly discussed herein in relation to its effect on CO oxidation.

In addition to these catalytic studies on the Pd surfaces, a large body of work (*30–33* and references contained therein) on the closely related SnO_x/Pt supported catalysts has suggested that surface hydroxyl species play a central role in promoting their activity toward CO oxidation. The presence of hydroxyl surface species is certainly a possibility on supported catalysts (especially those

calcined in air), but we have rigorously avoided the deliberate addition of H_2 or H_2O for several reasons. The rationales for this approach include: (a) focusing on the surface reactivity at purposely ordered surfaces with a minimum of poorly controlled parameters; and (b) we have no direct method of quantifying surface hydroxyl coverage either postmortem or during reaction conditions. In fact, recent high resolution electron energy loss studies following CO oxidation over Rh(111) (*34*) had revealed the existence of surface carbonate and hydroxyl intermediates. Future studies on the role of surface hydroxyl coverage as a function of reaction parameter space using techniques sensitive to $-OH$ coverage (e.g., secondary ion mass spectroscopy, high resolution electron energy loss spectroscopy, and Fourier transform infrared spectroscopy) would certainly be desirable.

2. EXPERIMENTAL

The experimental arrangement and conditions for all of the UHV techniques were essentially the same as described in a previous publication (*23*), with the addition of a high pressure (upper pressure limit 1000 Torr) microreactor. The UHV chamber and microreactor region have a base pressure of 2×10^{-10} Torr with a background gas contribution typical of baked stainless steel. Briefly summarizing the surface analytical experimental capabilities, the UHV chamber had provision for AES, LEED, and thermal desorption mass spectroscopy (TDMS). The Pd(100) crystal was prepared using conventional metallographic techniques as previously reported (*23*). Preparation and cleaning of the Pd(100) disk (~6 mm diameter) was achieved using conventional methods, and surface cleanliness was checked with AES and LEED (11). Sample temperatures were varied from 300 to 1200 K by use of a resistively heated sample mount arrangement. The starting point for our work was the $p(1 \times 1)$ Pd(100) surface. Overlayer Sn and CO coverages are defined in absolute units (1 monolayer = 1 ML) relative to the ideal termination of the bulk Pd(100) lattice surface atom density, which is equal to 1.38×10^{15} atoms cm^{-2}. Tin depositions were conducted on both surfaces of the disk as described previously (*23*), with the deposition rate constant to within 10%. The reproducibility of the deposition source was also checked by subsequent trial depositions onto the cleaned substrate at 300 K and was determined to be $\pm$ 10% over a 4–6 hr period by AES. Exposures are given in units of Langmuir (L), where 1L equal 1×10^{-6} Torr sec.

All gases were research grade and were used without further purification, except for cold trapping of condensible impurities with liquid nitrogen. It is particularly important to remove Fe and Ni carbonyls from research-grade reactant gases. Subsequently, CO and O_2 were expanded into the evacuated microreactor and the temperature of the crystal raised to the appropriate temperature for a time period required to give 0.5–5% conversion. A sample of the gas was then taken by expansion of the reacted mixture into an evacuated sampling cell (volume = 40 cm^3) with a 15-min equilibration time. Samples were then injected into a Hewlett-Packard 5710 gas chromatograph using a porapak R column, a methanizer, and a flame ionization detector. Output was directed to Spectra-Physics 4271 (Varian, Inc.) integrator for analysis. Results are presented as turnover frequency (TOF—number of molecules per site per second).

After the reaction products were sampled, the microreactor was evacuated by a molecular drag pump to $< 10^{-4}$ Torr. Further evacuation to 10^{-7} Torr was accomplished using a 150 l/s turbomolecular pump. A gate valve was then opened between the microreactor and the surface analysis chamber. Sample transfer time between the start of evacuation and analysis by LEED, AES, and/or TDMS was approximately 7 min; furthermore, the pressure in the surface analysis system never exceeded 2×10^{-9} Torr. No metals (Ni, Fe) resulting

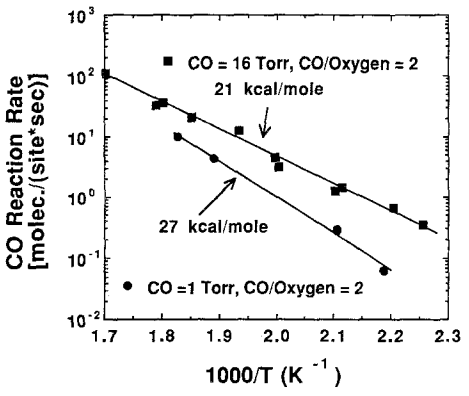

FIG. 2. Specific rates of reaction of CO (turnover frequencies) as a function of inverse temperature for the Pd(100) single crystal at total pressures of 24 and 1.5 Torr.

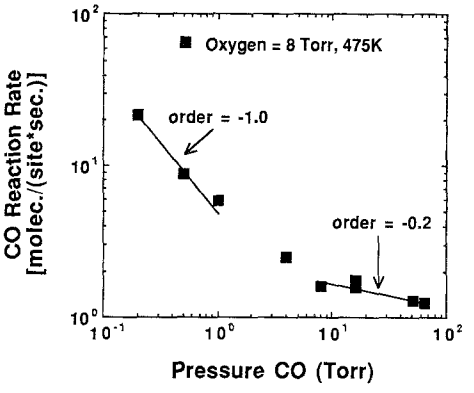

FIG. 3. CO partial pressure dependance for the Pd(100) single crystal surface at a constant O_2 pressure of 8 Torr and a temperature of 475 K.

from decomposition of carbonyls were observed by AES on the Pd(100) surface when using this procedure.

Reaction rates (as TOF) for CO oxidation were also checked on a Pt(100) single crystal disk and a polycrystalline Ta foil (99.999% Johnson–Matthey). The reactivity of the Pt(100) single crystal was found to match that reported by Berlowitz *et al.* (*11*), and the Ta was found to exhibit ≤ 1 pecent of the reactivity of the Pd(100) or the Pt(100) surfaces.

3. RESULTS

3.1 CO Oxidation at Pd(100)

Oxidation of CO was performed at the Pd(100) single crystal surface to establish a baseline for comparison with the Sn/Pd(100)-$c(2 \times 2)$ alloy. Figure 2 presents the turnover frequency (TOF) for CO as a function of inverse temperature. The data were obtained for the Pd(100) single crystal surface at 2 : 1 ratios of CO : O_2 and total pressures of 24 and 1.5 Torr, respectively. An increase in activation energy from 22 kcal/mole to 27 kcal/mole occurs as the total pressure drops. Furthermore, there is a corresponding decrease in the overall reaction rate as the total pressure is decreased.

The reaction rate dependence on the partial pressures of CO and O_2 were also studied on the Pd(100) surface (Figs. 3 and 4). These experiments were performed at constant temperature (475 K) and at fixed pressure of one of the reactants. The reaction rate order dependence on the pressure of CO (O_2 = 8 Torr) was found to change dramatically from -0.2 at pressures greater than 16 Torr to approximately -0.9 below 1 Torr. The reaction rate dependence in O_2 was also found to change with total pressure as shown in Fig. 4. It can be seen that the O_2 order varies from $+1.0$ at low total pres-

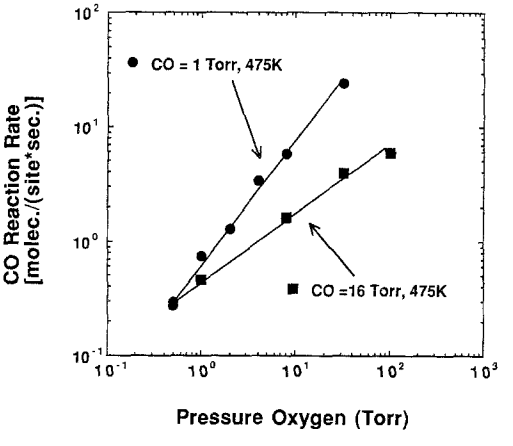

FIG. 4. O_2 partial pressure dependence for the Pd(100) single crystal surface at a temperature of 475 K and CO pressures of 16 and 1 Torr.

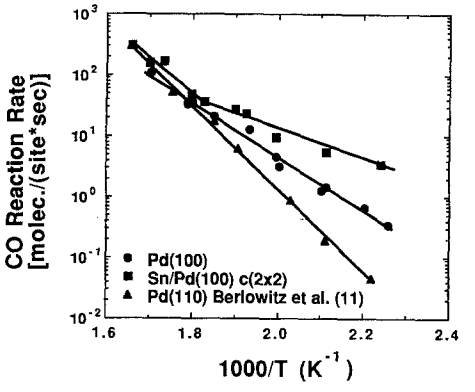

FIG. 5. Specific rates of reaction of CO (turnover frequencies) as a function of inverse temperature for the Pd(100) single crystal, Pd(110) single crystal (*11*), and $c(2 \times 2)$-Sn/Pd(100) surface alloy at a pressure of 24 Torr.

sures (CO = 1 Torr) to +0.6 at higher total pressures (CO = 16 Torr). Therefore, while the overall rate of reaction varies marginally with total pressure, the changes in the individual orders of reaction are quite significant.

3.2 CO Oxidation at the $c(2 \times 2)$-Sn/Pd(100) Surface Alloy

The $c(2 \times 2)$-Sn/Pd(100) bimetallic surface alloy was prepared and characterized by UHV techniques (AES, LEED) (*5*) prior to and after reaction. As shown previously, the idealized model of the $c(2 \times 2)$-Sn/Pd(100) surface alloy of Fig. 1 has a disposition of Sn and Pd surface atoms in a "checkerboard" pattern. This structure is thought to derive from the ideal termination (100) face of the Pd_3Sn bulk alloy (*26, 27*). The Pd_3Sn bulk alloy has been determined to be an FCC solid with a bulk lattice constant of 3.88 Å. This compares to 3.89 Å for the bulk Pd FCC lattice and suggests that the superlattice 1/2 order beams in the LEED pattern are due to the periodic two lattice space repeat distances seen in Fig. 1 (*5*). Identical LEED patterns and suggested surface alloys have also been prepared from the first and third row congeners (e.g., the (100) surfaces of Ni and Pt) (*5, 24*).

The CO oxidation reaction rate is plotted versus inverse temperature (P_{total} = 24 Torr, $CO:O_2$ ratio = 2) for the $c(2 \times 2)$-Sn/Pd(100) surface, the Pd(100) surface, and the Pd(110) surface (11) in Fig. 5. The activation energy for CO oxidation at the $c(2 \times 2)$-Sn/Pd(100) surface alloy was found to be 12 kcal/mole. This is a significantly lower activation energy than that of the Pd(100) single crystal surface (22 kcal/mole) and, furthermore, presents a much higher reaction rate even when based on the same number of sites as the Pd(100) single crystal. (Note that the TOF determination uses the same surface atom count for the Pd(100) crystal surface and the $c(2 \times 2)$-Sn/Pd(100) surface alloy and hence overestimates for Pd surface atoms in the latter by 2). Note, that above 540 K the slope for CO oxidation reaction on the $c(2 \times 2)$-Sn/Pd(100) surface alloy increases slightly to a value close to that observed on the Pd(100) surface. Figure 6 presents the reaction rate (as TOF) versus the CO partial pressure at a constant O_2 pressure of 8 Torr. It is immediately evident that the CO reaction order is greater than zero (+0.2). Furthermore, the reaction rate dependance on O_2 is also slightly positive (+0.1) (Fig. 7). These results are in stark contrast to those obtained at a Pd(100) single crystal surface and suggest that the physical

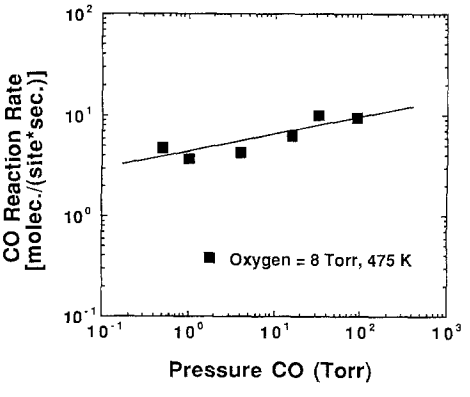

FIG. 6. CO partial pressure dependance for the $c(2 \times 2)$-Sn/Pd(100) surface alloy crystal surface at a constant O_2 pressure of 8 Torr and a temperature of 475 K.

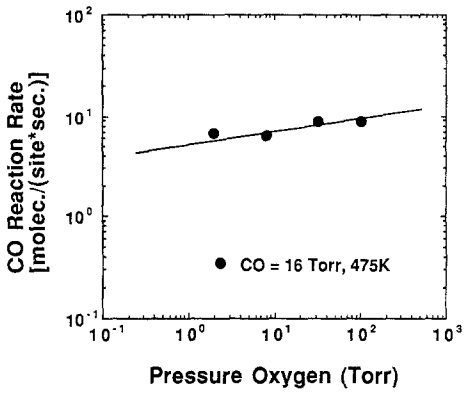

FIG. 7. O_2 partial pressure dependence for the $c(2 \times 2)$-Sn/Pd(100) surface alloy crystal surface at a constant O_2 pressure of 16 Torr and a temperature of 475 K.

parameters that influence the CO oxidation rate have markedly changed.

3.3 Post-reaction Surface Analysis (AES, LEED, TDMS) of Pd(100) and $c(2 \times 2)$-Sn/Pd(100)

Both the Pd(100) and the $c(2 \times 2)$-Sn/Pd(100) surfaces were characterized by AES, LEED, and TDMS following the microreactor catalytic reactions. The amount of CO remaining on the Pd(100) surface following reaction was estimated to be $\theta_{CO} = 0.5 \pm 0.1$ ML from comparison to saturation CO UHV exposure measurements on Pd(100). This value was determined by integrating the mass 28 TDMS traces for the respective surfaces. No significant CO_2 ($m/e = 44$) was observed during recording these TDMS traces, which is consistent with the prior observations of Berlowitz *et al.* (*11*) on post-CO oxidation reaction TDMS from Pd(110). However, LEED patterns consistent with complete splitting of the 1/2 order spots of the $c(2 \times 2)$ CO/Pd(100) LEED pattern corresponding to coverages of CO in the range of $0.55 \text{ ML} \leq \theta_{CO} \leq 0.65$ ML (as compared with those obtained by Tracy and Palmberg) were observed after reaction and upon cooling to room temperature (16 Torr CO and 8 Torr O_2) (*21*). The LEED patterns observed in this study are identical to those reported by Tracy and Palmberg, who monitored the isosteric adsorption of CO at pressures between 4×10^{-4} to 5×10^{-8} Torr and temperatures between 150 and 450 K (*21*). Although the amount of CO globally adsorbed on the Pd(100) surface following high pressure reaction is slightly less than saturation room temperature coverage using UHV CO dosing, some CO post-adsorption undoubtedly occurred during sample cooling and transfer. We, however, did not observe a LEED pattern from room temperature UHV saturation CO exposure on the clean Pd(100) surface (the crystal could not be cooled below 300 K). Evidently there are definitely ordered CO domains with local coverages of ≈ 0.6 ML. These domains of CO following reaction may be stabilized by very low amounts of impurity species (either adsorbed O atoms or unreacted OH species). Only a small oxygen AES signal ($\Theta_O < 0.05$ ML) was observed after reaction. Heating the crystal to 673 K restored the $p(1 \times 1)$ LEED pattern, and no oxygen remained in the subsequent AES spectrum.

Post-reaction examination of the $c(2 \times 2)$-Sn/Pd(100) surface alloy yielded only a very diffuse $p(1 \times 1)$ LEED pattern (at CO/O_2 ratios greater than 0.2), indicating that no large ordered domains of CO were present and that the $c(2 \times 2)$ surface had been disordered. The quantity of CO remaining on this surface following reaction was estimated by TDMS to be 0.114 ML. This CO coverage value was determined by comparison to the integrated mass 28 TDMS traces observed from Pd(100). No significant CO_2 ($m/e = 44$) was observed during the recording of these TDMS traces. The amount of oxygen (CO + O) on the surface was estimated by AES to be approximately 1 ML after reaction (referenced to the O AES signal observed for the $\Theta_O = 0.5$ ML structure seen on the O–$c(2 \times 2)$-Pd(100) surface). However, heating the substrate to 673 K lead to restoration of the $c(2 \times 2)$ pattern associated with Sn/Pd(100) surface alloy

with Θ_O = 0.05 ML still present, as determined by AES. Heating to temperatures above 673 K leads to partial removal of the surface Sn.

Exposure of the $c(2 \times 2)$-Sn/Pd(100) surface alloy to O_2 at 8 Torr for 1 min at 473 K yielded a 12-fold LEED pattern attributed to ordered SnO_2 atop Pd(100) (*5*). This pattern can be generated from two hexagons rotated 90° with respect to each other. One hexagon includes the 0,1 and 0,−1 substrate spots while the other hexagon includes the 1,0 and −1,0 substrate spots. An identical LEED pattern is observed following thermal desorption from or annealing the $c(2 \times 2)$-Sn/Pd(100) surface alloy after reaction ($CO/O_2 < 0.2$). The ability of the surface to absorb and react with CO was examined by thermal desorption from this ordered O/Sn/Pd(100) interface following a 1-L exposure of CO. This resulted in the desorption of CO_2 starting at approximately 400 K and only a slight decrease in the oxygen AES signal. Further cycles of CO adsorption/desorption (100-L exposures) produced no detectable CO_2 formation from TDMS measurements; however, a significant decrease in the CO peak desorption temperature from 450 to 350 K was seen. A 50% decrease in the AES oxygen signal is observed if the oxide surface is heated to 573 K and dosed with 10,000 L of CO (5×10^{-5} Torr, 200 s). These experiments confirm that the oxidized Sn/Pd(100) surface adsorbs CO at 300 K and is partially reducible at reaction temperatures of 573 K. In contrast, low coverages of O_a are obtained on the Pd(100) single crystal after high pressure (1–100 Torr) reaction with no CO_2 TDMS peak (m/e = 44) observed for the analogous experiments.

4. DISCUSSION

4.1 CO Oxidation at Pd(100)

The results presented here show that the Pd(100) single crystal surface has a noticeably different activation energy for CO oxidation than those previously reported for the Pd(110) surface (*11*). This is surprising in light of the previous studies (*13, 19*), which have concluded that the oxidation of carbon monoxide over Pd is structure-insensitive at temperatures greater than 475 K. Recently, Landry and Boudart reported a variation in activation energy as a function of pressue for the CO oxidation reaction on a supported Pd/Al_2O_3 catalyst (*13*); however, a detailed mechanistic interpretation of their results has yet to appear in print. Therefore, the original description of the CO oxidation reaction as a structure insensitive reaction may only be valid under specific conditions of low pressure (e.g., < 1 Torr). For example, the kinetic parameters derived for the CO oxidation reaction over Pd(100) show a specific trend in activation energy and orders of reaction (Figs. 2–4). For the Pd(100) surface the activation energy for the CO oxidation reaction decreases and the orders of reaction for CO and O_2 deviate from −1 and 1, respectively, as one increases the total pressure. However, this does not necessarily invalidate the L–H mechanism but merely points to changes in the rate-limiting step. This has been specifically addressed by Engel and Ertl (*20*), who pointed out numerous cases in which the coverage of CO or O affected the observed orders of reaction during CO oxidation studies under UHV conditions. A similar situation can therefore be envisioned in which severe coverage restraints during the CO oxidation reactions, at higher pressures, affect the observed orders of reactions on for supported Pd (*35*) or the Pd(100) single crystal used in this study.

Changes in the activation energies as a function of temperature for CO oxidation over Pd(110) have been explained in terms of changing CO coverages (*11*). The CO is thought to form a more compact structure on the Pd(110) surface as the temperature is lowered below 460 K and hence leads to a decreased CO binding energy. A similar situation is hypothesized to exist for the Pd(100) single crystal.

For the Pd(100) surface we make reference to the early work of Tracy and Palmberg (*22*). In their studies of CO adsorption/

desorption on Pd(100) they described the equilibrium between observed CO surface structures at an associated temperature and pressure using the Clausius–Clapeyron equation. Using this thermodynamic relationship and the conditions of this work (temperatures $\leq$ 580 K, pressure = 24 Torr) agreement between the structures that should be formed at these given pressures, the heats of adsorption of CO, and the measured activation energies for CO oxidation is obtained. In fact, reaction rates at a total pressure of 1.5 Torr are associated with CO coverages of close to 0.5 ML which have CO heats of adsorption of approximately 30 kcal/mole. At 16 Torr CO, the equilibrium CO surface structure is under increasing compression (due to increasing Θ_{CO}) at temperatures less than 635 K. For the reaction temperatures used in this study (443–600 K), the surface CO coverage is suggested to be associated with highly compressed structures ($\Theta_{CO} \geq 0.55$ ML) with a corresponding CO heat of adsorption of $\approx$ 22 kcal/mole. Such a value is in good agreement with the CO oxidation activation energy shown in Fig. 2. Infrared adsorption experiments should be able to address the coverage more explicitly under reaction conditions and will form the venue for future studies.

Exhaustive observations on the UHV reactivity of CO and O_a by Stuve *et al.* (*36*) on the Pd(100) surface have determined that CO adsorbs readily on a $p(2 \times 2)$-O/Pd(100) surface up to 0.8 ML. Furthermore, the $CO_{ad} + O_{ad}$ can be reacted off the surface as CO_2. A Pd–O–CO site was hypothesized to exist for the 0.8 ML CO–0.25 ML O surface which is highly reactive for CO_2 formation. The CO and O_2 reaction orders also provide a measure of a change in the overall CO_{ad} and O_{ad} coverages. It is postulated by Engel and Ertl (*20*) that the local O atom ($p(2 \times 2)$) structure formed on the Pd(111) single crystal surface can be compressed by the coadsorption of CO. Compression of the O atom islands with the adsorption of CO was found to cause a decrease in the overall Pd–O bond strength. On the other hand, increasing the CO coverage inhibits the dissociative adsorption of O_2 on both surfaces. Therefore, the observed high pressure reaction orders can be explained by the following rationale. At lower pressures (1 Torr CO or less), the CO oxidation reaction operates with no adsorption inhibition for the L–H mechanism due to compressed CO islands. However, at the higher pressures used in this study, compressed structures of CO will certainly block dissociative adsorption of O_2 molecules. This in effect produces a CO saturated surface that is less sensitive to increases in CO coverage and similarly causes the O_2 reaction order to decrease.

Similar changes in CO oxidation reaction orders for O_2 (1.0 to 0.6) and CO (-1.0 to -0.2) have been reported for supported Pd catalysts by Cant *et al.* (*12*) when the reaction temperature is lowered below 390 K. These findings with respect to kinetic parameters, therefore, suggest that the activation energies observed on the supported catalysts are influenced by three important factors: the relative distribution of (100), (110), and (111) sites; the reactant concentrations at which the reaction is carried out; and the increase in the CO coverage that occurs as the temperature is lowered.

4.2 CO Oxidation at the $c(2 \times 2)$-Sn/Pd(100) Surface Alloy

The $c(2 \times 2)$-Sn/Pd(100) bimetallic surface alloy presents a unique opportunity to understand the nonsupport related effects of alloying a second component. As mentioned previously, the chemical adsorption and reactivity difference of this surface alloy with respect to both CO and O_2 allow a direct comparison with the Pd(100) surface, since the previously studied identical single crystal surface was used to produce the $c(2 \times 2)$-Sn/Pd(100) surface alloy. It was seen in Fig. 5 that the CO oxidation rate is greatly enhanced by alloying Sn with the surface. This is quite surprising in light of the fact that UHV dosing of CO onto the surface results in no CO adsorption above room temperature at the $c(2 \times 2)$-Sn/Pd(100) sur-

face alloy (T_s = 300 K). For the latter surface, this is thought to arise from the elimination of Pd–Pd bridge binding sites (CO chemisorbs exclusively at bridge sites at all coverages on Pd(100)) by addition of Sn adatoms in forming the proposed "checkerboard" $Pd_3Sn(100)$ surface alloy (Fig. 1 and Ref. (*5*)). Oxygen exposures equivalent to reaction conditions ($\sim 5 \times 10^4$ Torr sec.) at the Sn/Pd(100) surface alloy results in a surface with the Sn component displaced out of the surface plane and is in effect a SnO_x ($x = 1-2$) overlayer (*5*). The SnO_x portion of the interface serves as a ready oxygen reservoir that facilitates reaction with CO adsorbed at defect and other sites in which a significant number of Pd atoms exist in close proximity. Above temperature of 540 K the CO oxidation rate at the $c(2 \times 2)$-Sn/Pd(100) surface alloy closely resembles the reactivity observed at the Pd(100) surface. This may be due to the catalytic contributions from several different sites at the bimetallic surface, with predominantly Pd sites comprising the bulk of the reactivity above 540 K.

The increase in the CO oxidation rate at the Sn/Pd(100) surface alloy is not without previous precedents. For example, Engel and Ertl (*20*) and Berlowitz *et al.* (*11*) found that an increase in the overall oxygen content of the surface increases the reaction rate on Pd. As previously stated, the Sn adatoms are pulled out of the surface plane by oxidation forming a partially oxidized overlayer (*5, 24*). The formation of this SnO_x overlayer presents a laterally heterogeneous surface to the reactant species. The reaction can then proceed through chemisorbed CO at either oxidized Pd (+2) or Sn (+2, +4) sites. The catalytic rate of CO oxidation over SnO_2 was previously investigated by Fuller and Warwick (*37*). The activation energy for CO oxidation over SnO_2 was found to be 17 kcal/mole and postulated to occur by a redox mechanism. They observed reaction rates that were entirely independent of the O_2 partial pressure, while the CO partial pressure order was observed to vary between 1 and 0 as the CO pressure increased. Work by Bond, Fuller, and Molloy (*16*) showed that Pd/SnO_2 catalysts have activation energies for CO oxiation as low as 11 kcal/mole and are significantly more active than SnO_2 alone. It was also pointed out by Bond *et al.* (*16*) that the order of reaction for CO was nearly zero, and the reaction order for O_2 decreased from 0.4 to 0.0 as the oxygen partial pressure was increased. This corresponds quite well with the observation that the activity of the SnO_2 is nearly 2 orders of magnitude lower (at the same temperature) than that of the $c(2 \times 2)$-Sn/Pd(100) surface alloy used in this study. They suggested that the small crystallites of Pd in intimate contact with the SnO_2 increased the CO oxidation rate by "spillover" of CO and O to the SnO_2 support. Alternatively, a similar mechanism might be occurring on islands of metallic Pd that are created during reaction. At such sites CO can adsorb and subsequently react with domains of oxide in close proximity. Recent studies by Baiker *et al.* (*38*) point to an enhanced CO oxidation reaction rate on oxidized PdZr alloys. In their work an amorphous solid solution of Pd, Zr, and O is thought to exist where an oxidized surface Pd atom binds CO and the Zr changes oxidation state by giving up an oxygen atom during the reaction to form CO_2. The creation of Lewis acid sites in the ZrO component of the PdZr supported alloy may be providing the necessary reactive sites for the reaction to proceed.

The CO oxidation kinetics at supported and unsupported Pt, Pd, and Rh foils have been studied by Yao (*39*). She observed two types of reaction kinetics for the CO oxidation reaction with two types of sites required for their interpretation. Standard L–H kinetics (Type 1) were observed for precious metal wires and exhibited a positive first-order dependance with respect to O_2 and a negative first-order dependance with respect to CO. These kinetic parameters were attributed by her to the low oxidation states of the metal. A second set of kinetic parame-

ters (Type 2) were obtained for highly dispersed precious metals on Al_2O_3 or CeO_2/Al_2O_3. These exhibited a positive order of reaction for CO and were nearly independent of the O_2 partial pressure. This suggests that the active metal site is a cation surrounded by oxygen anions and/or adsorbed oxygen. Furthermore, the CO oxidation activation energies observed for the Type 2 were found to be lower than those of the Type 1 kinetics (i.e., 10 kcal/mole versus 30 kcal/mole).

Therefore, the CO oxidation kinetics at the $c(2 \times 2)$-Sn/Pd(100) surface alloy appear to be similar to those observed on the small particle Pd/SnO_2 system (16), the Pd/Zr oxide system (*38*), and that of the highly dispersed Pt, Pd, and Rh systems in intimate contact with CeO_2 (*39*). The increased activity of a reducible oxide in intimate contact with a catalytically active noble metal has also been expounded at length in previous studies on the activity and characterization of supported SnO_x/Pt catalysts (*30–33*).

5. CONCLUSIONS

The activation energy for CO oxidation at the Pd(100) surface was measured at operating pressures from 0.3 to 180 Torr and found to be 22–27 kcal/mole over the temperature range 443–673 K. For this surface the reaction order for the CO was found to vary from -0.2 to -0.9 as the pressure was lowered from 16 to 1 Torr CO ($P_{O2} = 8$ Torr), and the O_2 reaction order was measured to vary from 0.6 to 1.0 at CO pressures of 16 and 1 Torr, respectively. These observations are in agreement with those previously reported for supported Pd/SiO_2 catalysts at low temperatures (*12*). This low activation energy is also consistent with the low value for the isosteric heat of adsorption of CO at Pd(100) at near saturation coverages ($\Theta_{CO} > 0.6$ ML).

The $c(2 \times 2)$-Sn/Pd(100) surface alloy displays enhanced CO oxidation rates compared to Pd(100) under identical reactant conditions. The activation energy for CO oxidation at the $c(2 \times 2)$-Sn/Pd(100) surface alloy is 12 kcal/mol at a total pressure of 24 Torr ($CO : O_2 = 2$). Furthermore, the orders of reaction for CO and O_2 are determined to be $+0.2$ and $+0.1$, respectively. Post-reaction surface analysis of the $c(2 \times 2)$-Sn/Pd(100) surface alloy by AES and LEED indicates that the Sn component preferentially oxidizes and results in an SnO_x overlayer. The reaction proceeds at a surface consisting of a layer of disordered SnO_x ($x = 1-2$) atop the Pd(100) template.

ACKNOWLEDGMENTS

Support by the Department of Energy through internal research funds at Los Alamos National Laboratory is gratefully acknowledged. We also thank Dr. C. H. F. Peden, Sandia National Laboratories–Albuquerque, for many helpful discussions during the preparation of this manuscript.

REFERENCES

1. Gavrilov, D. N., Musakin, G. A., and Fedorov, N. F., *Zh. Prikl. Khim.* **63,** 1125 (1990).
2. Kummer, J. T., *J. Phys. Chem.* **90,** 4747 (1986).
3. Engel, T., and Ertl, G., *Adv. Catal.* **28,** 1 (1979).
4. Engel, T., and Ertl, G., *in* "The Chemical Physics of Solid Surfaces and Heterogeneous Catalysts" (D. A. King and D. P. Woodruff, Eds.), Vol. 4. Elsevier, Holland, 1982.
5. Logan, A. D., and Paffett, M. T., *in* "Proceedings of the 12th North American Conference on Catalysis, Lexington, KY, April, 1991"; and submitted for publication.
6. Goodman, D. W., *Annu. Rev. Phys. Chem.* **37,** 425 (1986).
7. Campbell, C. T., *Annu. Rev. Phys. Chem.* **41,** 1 (1990).
8. Stephens, S. J., *J. Phys. Chem.* **63,** 188 (1959).
9. Alexander, E. G., and Russell, W. W., *J. Phys. Chem.* **68,** 1614 (1964).
10. Kawasaki, K., Sugita, T., and Ebisawa, S., *J. Chem. Phys.* **44,** 2313 (1965).
11. Berlowitz, P. J., Peden, C. H. F., and Goodman, D. W., *J. Phys.Chem.* **92,** 5213 (1988).
12. Cant, N. W., Hicks, P. C., and Lennon, B. S., *J. Catal.* **54,** 372 (1978).
13. Landry, S. M., and Boudart, M., *J. Phys. Chem.* **94,** 1203 (1990).
14. Ladas, S., Poppa, H., and Boudart, M., *Surf. Sci.* **102,** 151, (1981).
15. Stark, D. S., and Harris, M. R., *J. Phys.* **16,** 225 (1983).
16. Bond, G. C., Molloy, L. R., and Fuller, M. J., *J. Chem. Soc., Chem. Commun.* **19,** 796 (1975).
17. Palazov, A., Kadinov, G., Bonev, Ch., Dimitrova, R., and Shopov, D., *Surf. Sci.* **225,** 21 (1990).

18. Langmuir, I., *Trans. Faraday Soc.* **17,** 621 (1921–1922).
19. Ertl, G. and Koch, J., *in* "Proceedings of the 5th international Conference on Catalysis, Palm Beach, 1972" (J. W. Hightower, Ed.), p. 969. North-Holland, Amsterdam, 1973.
20. Engel, T., and Ertl, G., *J. Chem. Phys.* **69,** 1267 (1978).
21. Conrad, H., Ertl, G., Koch, J., and Latta, E. E., *Surf. Sci.* **43,** 462 (1974).
22. Tracy, J. C., and Palmberg, P. W., *J. Chem. Phys.* **31,** 4852 (1969).
23. Paffett, M. T., and Windham, R. G., *Surf. Sci.* **208,** 34 (1989).
24. Paffett, M. T., Logan, A. D., Simonson, R. J., and Koel, B. E., *Surf. Sci.,* in press.
25. Overbury, S., Bertrand, P., and Somorjai, G., *Chem. Rev.* **75,** 547 (1975).
26. Hansen, M., "The Constitution of Binary Alloys," McGraw–Hill, NY, 1958.
27. JCPDS International Centre for Diffraction Data, "Powder Diffraction File," p. 37. Swarthmore, PA, 1988.
28. Overbury, S., Mullins, D., Paffett, M. T., and Koel, B. E., *Surf. Sci.,* **254,** 45 (1991).
29. Biberian, J. P., and Van Hove, M. A., *Surf. Sci.* **118,** 443 (1982).
30. Schryer, D. R., Upchurch, B. T., Hess, R. V., Wood, G. M., Sidney, B. D., Miller, I. M., Brown, K. G., Van Norman, J. D., Schryer, J., Brown, D. R., Hoflund, G. B., and Herz, R. K., *in* "Low Temperature CO-Oxidation Catalysts for Long-Life CO_2 Lasers," (D. R. Schryer and G. B. Hoflund, Eds.), Publication 3076, p. 41. 1990.
31. Hoflund, G. B., Grogan, A. L., Asbury, D. A., and Schryer, D. R., *Thin Solid Films* **169,** 69 (1989).
32. Gartner, S. D., Hoflund, G. B., Davidson, M. R., and Schryer, D. R., *J. Catal.* **115,** 132 (1989).
33. Gardner, S. D., Hoflund, G. B., Schryer, D. R., and Upchurch, B. T., *SPIE Proc.* **1062,** 21 (1989).
34. Peden, C. H. F., and Houston, J. E., *J. Catal.* **128,** 405 (1991).
35. Choi, K. I., and Vannice, M. A., *J. Catal.,* **131,** 1 (1991).
36. Stuve, E. M., Madix, R. J., and Brundle, C. R., *Surf. Sci.* **146,** 155 (1984).
37. Fuller, M. J., and Warwick, M. E., *J. Catal.* **29,** 441 (1973).
38. Baiker, A., Gasser, D., Lenzner, J., Reller, A., and Schlogl, R., *J. Catal.* **126,** 555 (1990).
39. Yu Yao, Y.-F., *J. Catal.* **87,** 152 (1984).